Materials Research. 2025; 28:e20240257
DOI: https://doi.org/10.1590/1980-5373-MR-2024-0257

Silica Deposition on Polyamide 6,6 Fabrics by Hybrid Corona-Dielectric Barrier Discharge Plasma

Isabella Grinberg Francelino[a], *Felipe de Souza Miranda*[a,b], *Fernando Gasi*[c]*, *Marcia Cristina Silva*[c], *Sérgio Ricardo Lourenço*[c], *Gilberto Petraconi Filho*[a]

[a]*Instituto Tecnológico de Aeronáutica (ITA), São José dos Campos, SP, Brasil.*
[b]*Universidade Estadual Paulista (Unesp), São José dos Campos, SP, Brasil.*
[c]*Universidade Federal do ABC (UFABC), São Bernardo do Campo, SP, Brasil.*

Received: June 03, 2024; Revised: August 09, 2024; Accepted: September 18, 2024

This work aims to deposit silica (SiO_2) on polyamide 6,6 fabrics by hybrid corona-dielectric barrier discharge plasma at atmospheric pressure. The reactor used, developed at the Laboratory of Plasma and Processes of the Aeronautics Institute of Technology (LPP/ITA), allows the treatment of fabric surfaces by activation and plasma deposition processes, aiming, in this order, the alteration of wettability and the deposition of silica on its surface, using a silicic acid solution ($Si(OH)_4$) as a silica precursor. The morphology of the deposited films was evaluated by scanning electron microscopy (SEM). To identify the chemical modifications generated by the plasma treatment, the untreated and treated samples were analyzed by Fourier transform infrared spectroscopy with attenuated reflectance (FTIR-ATR) and Energy Dispersive Spectroscopy (EDS). The thermal behavior of the treated and untreated samples was evaluated by Differential scanning calorimetry (DSC) and thermogravimetric analysis (TGA). Additionally, X-ray diffraction (XRD) was also used to identify crystalline phases in the film. The results showed that plasma processing proved to be an effective technique for modifying the surface characteristics of polyamide 6,6.

Keywords: *Silica, polyamide 6,6, deposition, corona-dielectric barrier discharge, silicic acid.*

1. Introduction

SiO_x films are very attractive for different applications, such as optical coatings, corrosion protection and food and pharmaceutical packing[1]. SiO_2 thin films exhibit exceptional optical properties, such as high transparency and low refractive index, which can reduce reflection and avoid light scattering. Additionally, these films demonstrate low absorption in the visible and near-infrared wavelength spectrum[2]. Moreover, SiO_2 films can enhance heat resistance, augmenting their utility in various applications[3].

The literature has reported that SiO_2 thin films have been synthesized using different methods[4]. One of the most used methods is using hexamethyldisiloxane (HMDSO) monomer in SiO_x and SiO_2 films deposition in atmospheric and low pressure[5]. Other techniques, named wet processes, are based on chemicals and generate chemical waste[6].

Although low-pressure plasma treatments allow greater stability, control, and reproducibility of the process[7], the need to create and sustain low-pressure conditions limits energy efficiency and productivity, making it unattractive for industrial applications. The use of non-thermal cold plasmas operating at atmospheric pressure, on the other hand, makes it possible to obtain a similar surface treatment in a continuous process and with a reduction in processing cost[8,9].

Different research groups are reporting significant advances in this scope[10]. Some techniques used for thin film deposition on atmospheric pressure include the dielectric barrier discharge (DBD), the corona discharge, the atmospheric pressure plasma jet (APPJ), and the atmospheric pressure glow discharge (APGD)[11].

Using non-thermal cold plasmas operating in atmospheric pressure makes it possible to modify textiles' surface properties, without altering their bulk properties[11]. These plasmas are suitable for this application, because most textiles are heat-sensitive polymers[12]. One advantage of the plasma treatment of textiles is that it is an eco-friendly alternative to other techniques. Furthermore, the treatment time of just a few seconds, in most cases, reduces energy consumption, reducing costs[6].

In general, non-thermal cold plasma treatment of polymers produces significant changes in the surface of the material, due to alterations in the chemical composition, molecular weight and morphology of the surface layer by the interaction of reactive species with the surface[13-15]. Using this technique, it is possible to obtain, for example, an increase in wettability, coating adhesion, printability, induced hydrophilic and hydrophobic properties, modification of electrical and/or physical properties and surface disinfection of the fibers. Furthermore, this technique allows surface modifications in extensive areas and with good uniformity[12].

*e-mail: gasifernando@gmail.com

In addition, through the plasma deposition process, thin films and functionalizing nanostructures can be deposited on the surface of textiles[16,17].

The mechanisms of silica deposition by plasma are not yet fully understood. Therefore, many researchers are working to identify the main silica precursor reactions, both in the gas phase (plasma-precursor interaction) and in the solid or condensed phase (plasma-surface interaction)[18].

According to Fanelli et al.[19], the general mechanism consists of an initial reaction step, where the activation of the precursor occurs by collision of electrons and/or reaction with the excited species to produce the primary reactive fragments. Primary and secondary fragments can undergo heterogeneous reactions in the solid phase (gas-surface interaction), contributing to film growth, and homogeneous reactions, such as oligomerization, leading to powder formation. Primary fragments can also undergo homogeneous oxidation in the gas phase to form partially and fully oxidized secondary fragments. Partially oxidized oligomers and fragments can also contribute to film growth, while powders can deposit both in the discharge and in the post-discharge region.

According to Cacot et al.[20], the precursor droplets quickly become charged when exposed to a DBD, and electrostatic forces control the movement of the droplets, leading to the deposition of a thin film on the substrate. In this process, it is assumed that droplets inserted into the DBD acquire a uniformly distributed charge over the surface. However, spatially inhomogeneous charging of the precursor droplets may occur, modifying the balance between the liquid's internal surface tension and external electrostatic and pressure forces. Thus, the droplet can become unstable, forming smaller droplets, which can subsequently be deposited on the substrate.

Therefore, this work reported the deposition of SiO_2 films on polyamide 6,6 (PA6,6) fabrics using a hybrid corona-dielectric barrier discharge treatment reactor. The reactor works at atmospheric pressure and uses silicic acid as a precursor of SiO_2. The silicic acid is used as a cheaper replacement for HMDSO. This precursor is nebulized directly to the plasma region through a flat cavity along the length of the high-voltage electrode. PA6,6 fabric was chosen for plasma treatment due to its physical and chemical properties and diversity of applications, such as in the aeronautical industry, medical textiles and high-performance fabrics.

2. Materials and Methods

2.1. Plasma treatment of PA6,6

The PA6,6 fabrics were treated by a hybrid corona-dielectric barrier discharge plasma operating in atmospheric pressure. Figure 1 presents a schematic drawing of the reactor.

The fabric was sewn into a cylindrical shell measuring 15 cm in height and 20 cm in diameter, matching the dimensions of the substrate-sample holder. The dielectric material was a silicone-based composite that endures temperatures up to approximately 300°C. The distance between the high-voltage electrode and the sample was adjusted to 1.5 mm. This specific distance was determined experimentally, primarily assessing a range where the discharge maintains good spatial uniformity.

The experimental setup also includes a nebulizer system, used in the plasma deposition process. For the silica film deposition, the silicic acid solution was nebulized directly into the plasma region through an open flat cavity (0.2 mm wide and 150 mm long) in the high-voltage electrode, as shown in Figure 1. In this process, the catalysis of plasma chemical reactions occurs in the gas or vapor and condensed phases. In the gaseous or vapor phase, the gaseous or nebulized precursor is inserted inside the hollow high-voltage electrode, which heats up with the application of the discharge power, raising the temperature in the region of reaction processes, which is also assisted by the ionization of the precursor through hollow cathode micro-discharges that expand both inside the electrode (plasma-precursor interaction) and outside, forming microjets of hollow electrode plasma towards the surface of the textile. In the condensed phase, the precursor plasma interacts directly with the textile surface (plasma-surface interaction). The associated regimes of DBD, corona and micro discharges improve the speed of chemical reactions and, consequently, the rates and selectivity of these reactions, reducing treatment time, process temperature, and reaction energies, increasing the energy efficiency of the process[22].

The samples were rotated, passing through the plasma region twice during the activation process in air plasma and four times during the deposition process. After plasma treatment, the treated samples were stored in vacuum-sealed plastic bags for subsequent characterization and comparison with the untreated sample.

2.2. Electrical characterization of the discharge

The electrical measurements were made using a Keysight digital oscilloscope model DSOX1202A, a Tektronix 1000:1 high voltage probe model P6015A, and an Agilent 10:1 probe model N2863B. The described apparatus allows a high definition of the pulses generated in the discharge in the electric current curve.

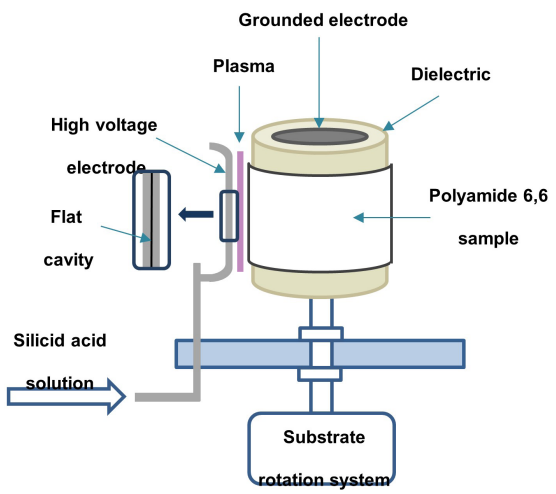

Figure 1. Schematic drawing of the process region of the plasma reactor. Adapted from[21].

The average discharge power (P) was calculated as shown in Equation 1.

$$P = \frac{1}{T}\int_0^T i(t).v(t)\,dt \quad (1)$$

where $i(t)$ and $v(t)$ are the current and the voltage as functions of time, respectively, and T is the period of the sinusoidal signal[23].

2.3. SiO_2 films

For the deposition of silicon dioxide (SiO_2) on the polyamide fabric, a solution of silicic acid ($Si(OH)_4$) was used as a precursor[24]. The solution was obtained using 10% by weight of aqueous sodium metasilicate ($Na_2SiO_3 \cdot 5H_2O$) through an ion exchange resin (IR-120; Rohm and Haas), the Si concentration of the solution was 0.5 mol/L[24-26].

2.4. Morphological and chemical characterizations of the samples

Scanning Electron Microscopy (SEM) was employed to observe changes in the sample structures. At the same time, energy-dispersive spectroscopy (EDS) helped identify chemical changes following silica deposition using the Tescan/Mira 3 microscope.

Fourier Transform Infrared Spectroscopy with Attenuated Reflectance (FTIR-ATR) was also utilized to detect chemical alterations before and after the deposition, using Perkin Elmer's Spectrum Spotlight 400 in ATR mode. The spectra were collected in transmission mode, with 64 scans per spectrum at a 4 cm^{-1} resolution, analyzing a frequency range from 4000 cm^{-1} to 400 cm^{-1}.

2.5. Wettability

Contact angle measurements were carried out at room temperature with deionized water. A Ramé-Hart 590 goniometer was used. Drops of (6.0 ± 0.1) µL were deposited with a syringe on the PA6,6 samples. The contact angle value was measured as the average of twenty consecutive measurements. DROPimage Advanced software was used for data acquisition.

2.6. Thermal analysis

Differential scanning calorimetry (DSC) and thermogravimetric analysis (TGA) techniques were used to evaluate the thermal behavior of the samples. DSC analysis was carried out on samples of approximately 10 mg in a Netsch DSC 404 C equipment from 30 to 300°C at a heating rate of 10°C/min, in a helium gas atmosphere. TGA analyses were made in a Netsch equipment model STA 449 F3 for samples of 9 mg from 30 to 600°C at a heating rate of 10°C/min in synthetic air atmosphere.

2.7. Microstructural characterization

X-ray diffraction (XRD) technique was used to identify crystalline phases in the film. The analyses were performed on a Rigaku model Ultima IV diffractometer. Monochromatic CuKα radiation (λ = 1.5406 Å, 40 kV and 30 mA) was used with θ/2θ geometry, in the range $10° < 2\theta < 80°$, angular step of 0.01° and angular speed of 5°/min.

3. Results and Discussion

3.1. Electrical characterization of the discharge

For the electrical characterization of the laboratory scale reactor discharge, a duty cycle voltage with a sinusoidal waveform with 11.5 kV amplitude and frequency of 23 kHz was applied as shown in Figure 2. Current analysis shows a typical profile of a DBD. The presence of silicic acid solution in air plasma intensifies the increase in the number of current peaks. The power of the air plasma was estimated at 10 W and after the introduction of silicic acid the power is increased to approximately 12 W. This increase in power occurs due to the increase in the electrical conductivity of the gap as a result of the presence of nebulized silicic acid, changing, therefore, the discharge impedance.

3.2. Morphological and chemical characterizations

3.2.1. Activation process

SEM images of the untread and plasma-activated samples are shown in Figure 3. It is observed that there was a significant change in surface morphology after plasma treatment. According to the literature, this change in morphology is driven by the impact of highly energetic and reactive plasma species. In addition to the increase in

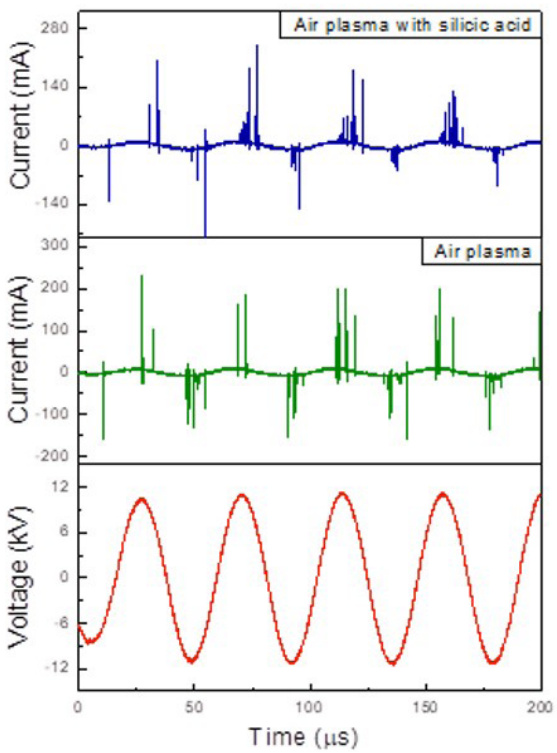

Figure 2. Applied voltage and discharge current of the laboratory-scale reactor operating at 23 kHz.

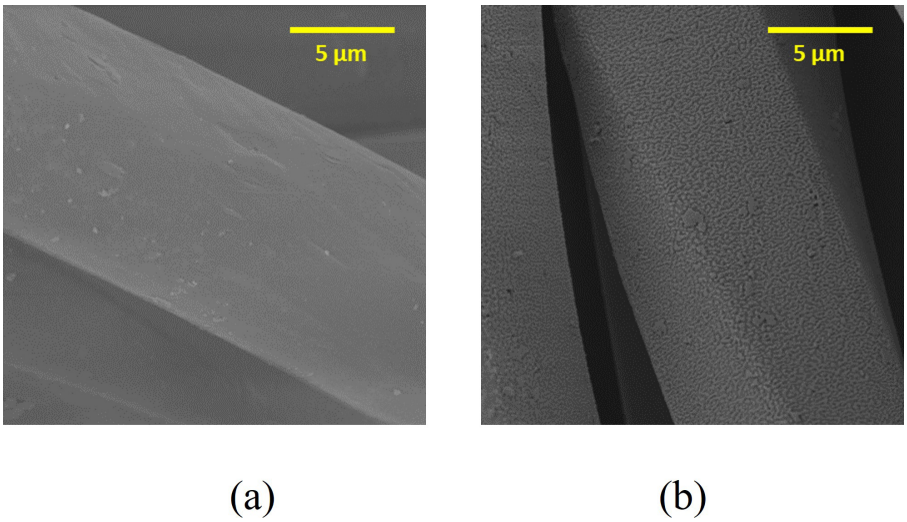

Figure 3. SEM images: (a) untreated sample; (b) plasma activated sample.

roughness, a break in the polymer chains may also occur, producing new functional groups or reorganizing existing polymer groups[27].

3.2.2. Silica deposition process

Figure 4 shows the SEM images of the treated samples for 2, 4, 6 and 8 passages in the silica deposition process.

The SEM images shown in Figure 4 indicate the formation of silica clusters well distributed on the surface of the fibers. Furthermore, cracks were observed in the coatings after 6 passes in the deposition process (Figure 4e-h). These cracks may result from greater sample heating due to the longer exposure time to the plasma. The difference between the thermal expansion coefficients of the coating and the substrate can cause tension to accumulate in the film, which relieves this tension when cracking[28,29]. Another possibility for the appearance of cracks in the coatings is the formation of a thicker film for a greater number of passes. According to Hegemann[30], thick coatings cause an accumulation of tension at the film/substrate interface, leading to the formation of cracks.

The formation of spherical clusters may be associated with interaction forces between the nanoparticles. In the droplets formed in the nebulization process, the nanoparticles are subject to Brownian motion and can interact with each other. When the liquid evaporates, the nanoparticles bond and move closer together, forming clusters. Parameters such as temperature gradients in the droplets and particle-particle interactions influence the final size and shape of the clusters[31].

Using the backscattered electron detector (BSE) of the scanning electron microscope, it is possible to detect the difference in the atomic number of the chemical elements present in the sample as a function of contrast. Figure 5 shows an image obtained using this detector for the sample which was treated with 8 passages in the silica deposition process. The contrast between the fiber and the coating indicates that they are composed of different elements, proving that there was silica deposition with coatings of 1 µm, estimated by the dimension scale shown in the image.

The EDS spectra of PA6,6 samples without treatment, with silica are presented in 6. These spectra indicate the presence of silicon (Si) in the treated samples. Peaks attributed to carbon (C), oxygen (O) and nitrogen (N), which are constituent elements of PA6,6, and gold (Au), due to the metallization of the samples carried out before analysis, are also observed. The weight percentages (wt%) of each element present in the samples and the respective standard deviation (σ) values for each of the spectra obtained are also shown in Figure 6.

Figure 7 shows the FTIR spectrum of the treated and untreated samples. The FTIR-ATR spectrum of untreated polyamide, corresponding to the red line in Figure 7, shows the inherent band of PA6,6 at 3300 cm^{-1} attributed to N−H stretching vibrations. The peaks at 2932 and 2860 cm^{-1} are related to the CH_2 asymmetric and symmetric stretching vibrations, respectively, while the absorption band at 1632 cm^{-1} is attributed to the C=O carbonyl stretching vibration of the secondary amide band. The band at 1533 cm^{-1} can be attributed to the N−H flexion movement and the band at 683 cm^{-1} to the O=C−N group[32].

According to the literature, the bombardment of ions (N_2^+, N^+, O_2^+, H_2O^+, O_2^- and O^-) induced by a plasma discharge can cause the breaking of bonds with energy less than 10 eV in the outer layers of the polymer, especially in the C−N bonds, which is the weakest bond in the polymeric chain[32]. The spectrum of the polyamide fabric has two characteristic crystalline peaks at 934 cm^{-1} due to axial deformation of the C–C=O amide and at 1198 cm^{-1} due to out-of-plane symmetrical angular deformation. Plasma treatment altered peak intensities in these regions, indicating significant changes in the crystallinity and structure of C−C bonds.

The black line in Figure 7 shows peaks resulting from Si–O stretching vibrations in the region of 940-1140 cm^{-1}[14,33]. A greater intensity of Si–O elongation peaks is observed at 1058 cm^{-1} after the plasma deposition process, indicating an increase in the concentration of nanosilica on the fabric surface.

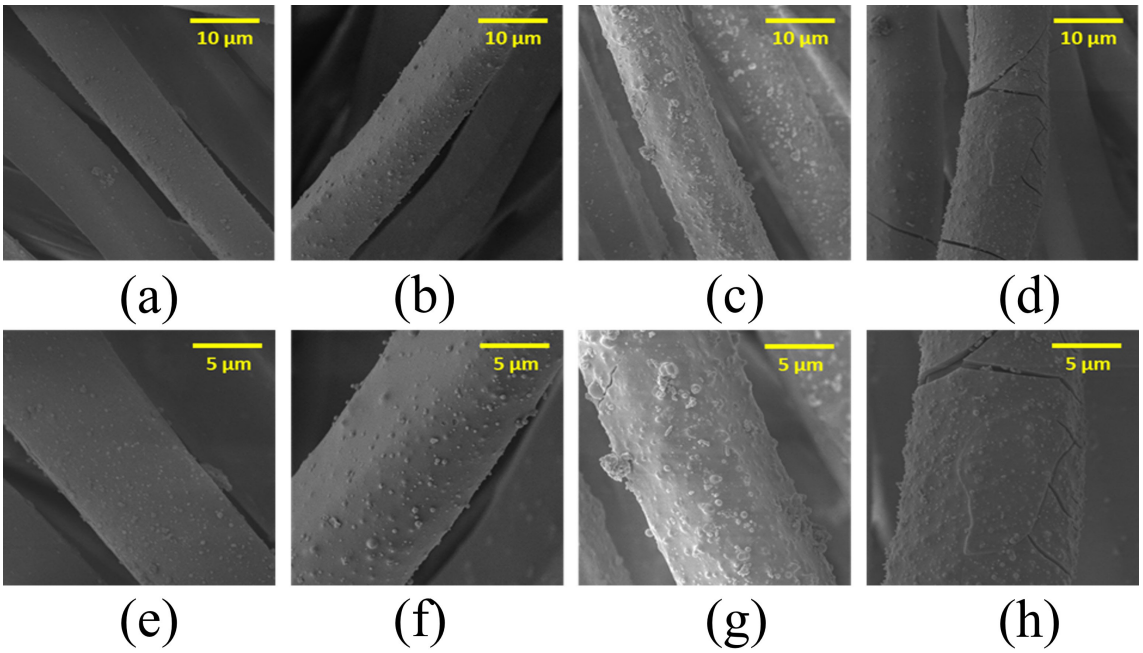

Figure 4. SEM images of the treated samples for (a,b) 2, (c,d) 4, (e,f) 6, and (g,h) 8 passages in the silica deposition process at a discharge power of 12 W (plasma dosages of 615 W.min.m^{-2}, 1230 W.min.m^{-2}, 1845 W.min.m^{-2} and 2460 W.min.m^{-2}, respectively).

3.3. Wettability

3.3.1. Activation process

After performing surface activation of the PA6.6 fabrics, the sample remained in a conditioned environment without vacuum preservation to measure the variation in the contact angle over time. Zero time corresponds to the time from which it is possible to evaluate the contact angle, since, immediately after air plasma treatment, the surface is super hydrophilic with zero contact angle. This analysis aimed to evaluate the effect of plasma treatment on the wettability of the sample, using aging time as a parameter. Figure 8 shows the variation of contact angle with time over 4 hours.

The results show that the non-activated sample has a hydrophobic surface with a contact angle of 120°. In contrast, the plasma-activated sample became hydrophilic, with a contact angle of 34° being measured at time zero. The effect of decreasing the contact angle can be attributed to the incorporation of polar groups on the surface of the fabric and the increase in roughness generated on the surface of the material due to the interaction of the plasma with PA6.6[21,27]. After 1 hour, the samples maintained a contact angle of 34°. Between 2 and 4 hours after time zero, the samples partially recovered their contact angle, reaching values of up to 60°. The increase in the contact angle hours after the activation process is related to the mobility of the polymer chains, which allows the surface to be restructured hours after plasma treatment[34-36].

3.3.2. Silica deposition process

For samples treated with 2 and 4 passages in the silica deposition process, contact angles of 120.2° and 118.3°, respectively, were measured (Figure 9), revealing a hydrophobic

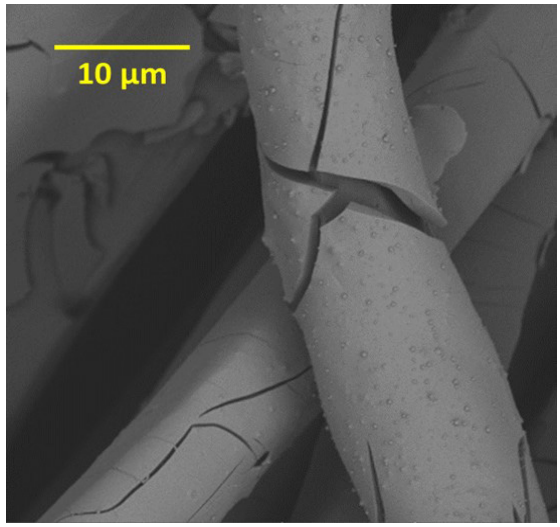

Figure 5. SEM image obtained using the backscattered electron (BSE) detector for the sample treated with 8 passages in the silica deposition process.

character. It is noteworthy in this case that the hydrophobic character is not changed to the sample without activation and deposition treatment. The contact angle was impossible to measure for samples treated with 6 and 8 passes in the silica deposition process as the fabrics absorbed the water droplet instantly, indicating that the fabrics had become hydrophilic. According to the SEM images of these samples (Figure 4e-h), the coatings present cracks, which can facilitate the penetration of water through the coating, justifying the observed hydrophilic behavior[37].

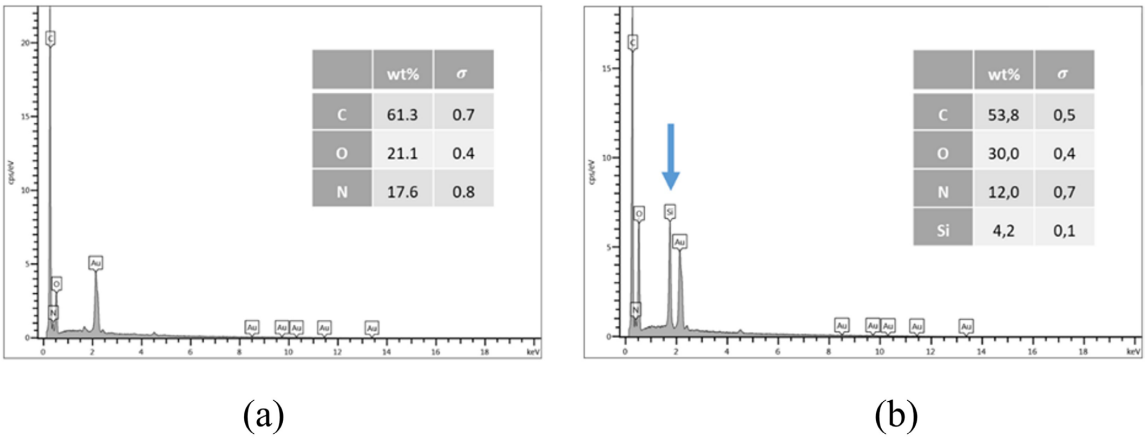

Figure 6. EDS analysis of the (a) untread sample and (b) the sample containing SiO_2.

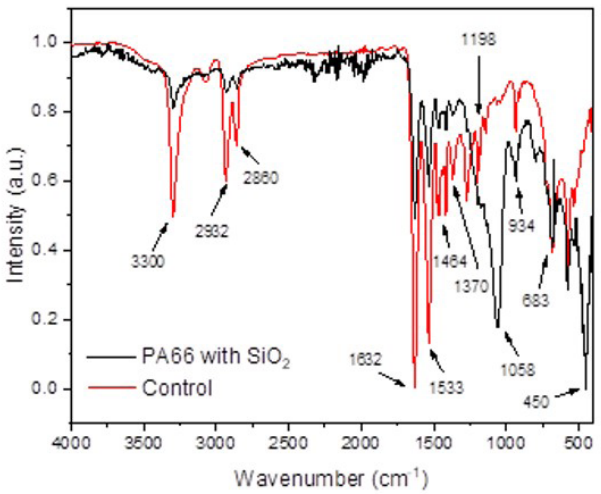

Figure 7. Infrared spectrum of the control sample (without treatment) and the sample coated with SiO_2 thin film via plasma.

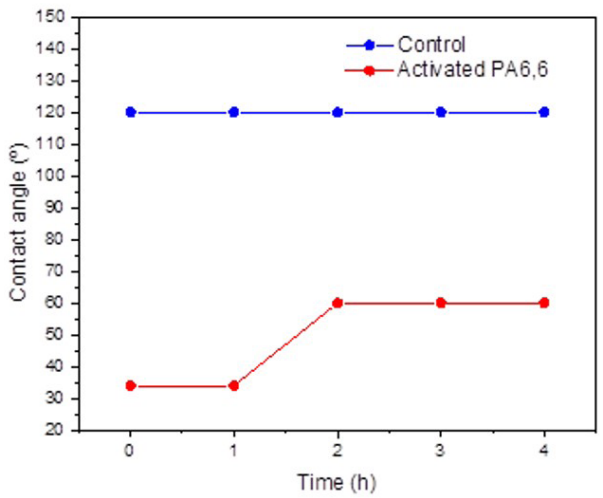

Figure 8. Contact angle as a function of aging time of the air plasma-activated PA6.6 fabric. The untreated sample has a contact angle equal to 120°; it is hydrophobic.

3.4. Thermal analysis

The DSC and TGA techniques were used to evaluate the thermal behavior of the untreated sample and the sample containing silica treated with 8 passages in the deposition process. The DSC results are shown in Figure 10. The presence of coatings on the fabrics had no effect on the melting temperature, as indicated by the peaks at 255.0°C in Figure 10.

The TGA results are shown in Figure 11. All samples demonstrated a similar mass loss trend, showing a stable mass up to approximately 350°C and greater decomposition between 350°C and 450°C. For the treated sample, a percentage

Figure 9. Contact angle of samples treated with (a) 2 and (b) 4 passages in the silica deposition process.

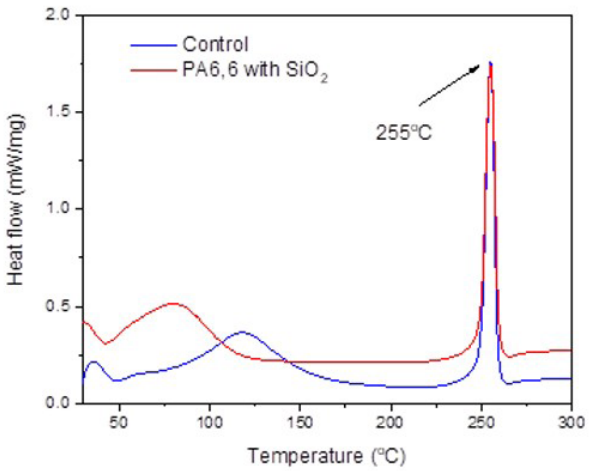

Figure 10. DSC analysis during heating of control sample and treated sample containing silica (8 passages in the deposition process).

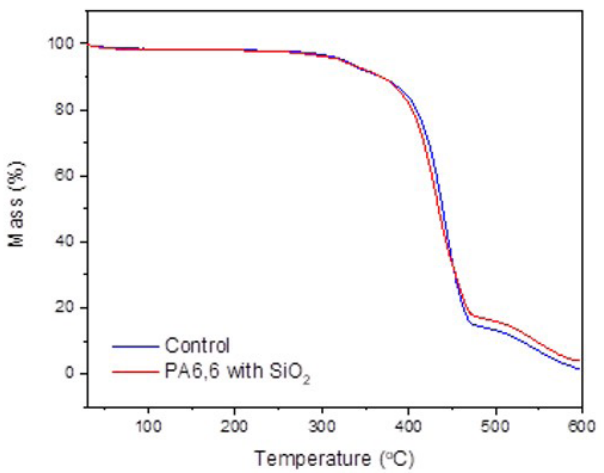

Figure 11. Thermogravimetric analysis of control sample and treated sample containing silica (8 passages in the deposition process).

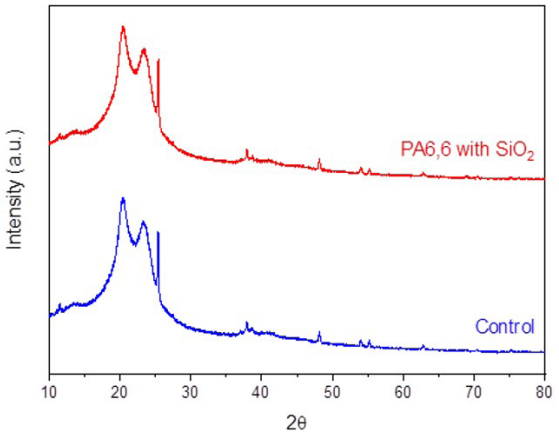

Figure 12. X-ray diffractograms of the control and treated sample (containing SiO_2).

of mass remains at the end of the analysis. This percentage possibly corresponds to the silica coating present in the fabric.

3.5. Microstructural characterization

Figure 12 shows the X-ray diffractograms of the untreated sample (control) and the sample containing silica treated with 8 passages in the deposition process. The diffraction patterns of the samples indicate a predominantly amorphous material with some crystallinity[38]. Differences in the intensity and positioning of the peaks between the diffractograms of the treated sample and the control sample were not observed, possibly due to the formation of very small crystals or amorphous coatings.

The characteristic peaks at 20.4° and 23.3° correspond to the (100) and (010)/(110) planes of the α phase, respectively. The first is attributed to the spacing between adjacent PA6,6 chains, which interact through hydrogen bonds, while the second is related to the distance between the polymer lamellas[38].

4. Conclusions

The findings from this study highlight the efficacy of employing hybrid corona-dielectric barrier discharge plasma at atmospheric pressure as a viable technique for surface modification of polyamide 6,6 fabrics. Through the activation process in air plasma, significant reductions in water contact angle and notable increases in surface roughness were observed. These modifications indicate an enhanced wettability, attributed to the enlarged contact area due to increased surface roughening. Furthermore, the technique's capability for silica deposition was corroborated through the analysis using FTIR-ATR and SEM imaging. In addition to its technical efficacy, the hybrid corona-dielectric barrier discharge plasma technique presents itself as a sustainable alternative to conventional surface treatment methods employed by the textile industry. Moreover, the successful modification of polyamide 6,6 fabric surfaces broadens the spectrum of innovation within the textile industry, enabling the development of new products with enhanced functionality and performance for a wide range of applications.

5. References

1. Omran AV, Pulpytel J. Cell-adherent SiO × coatings developed by an atmospheric transporting discharge [Internet]. 2018 [cited 2024 June 3]. Available from: www.begellhouse.com
2. Mazur M, Wojcieszak D, Kaczmarek D, Domaradzki J, Song S, Gibson D, et al. Functional photocatalytically active and scratch resistant antireflective coating based on TiO_2 and SiO_2. Appl Surf Sci. 2016;380:165-71. http://doi.org/10.1016/j.apsusc.2016.01.226.
3. Varnagiris S, Tuckute S, Lelis M, Milcius D. SiO_2 films as heat resistant layers for protection of expandable polystyrene foam from flame torch-induced heat. J Thermoplast Compos Mater. 2018;31(5):657-67. http://doi.org/10.1177/0892705717718238.
4. Schmidt-Szalowski K, Rżanek-Boroch Z, Sentek J, Rymuza Z, Kusznierewicz Z, Misiak M. Thin films deposition from hexamethyldisiloxane and hexamethyldisilazane under Dielectric-Barrier Discharge (DBD) conditions. Plasma Polym. 2000;5(3-4):173-90. http://doi.org/10.1023/A:1011314420080.
5. Schäfer J, Hnilica J, Šperka J, Quade A, Kudrle V, Foest R, et al. Tetrakis(trimethylsilyloxy)silane for nanostructured SiO_2-like films deposited by PECVD at atmospheric pressure. Surf Coat Tech. 2016;295:112-8. http://doi.org/10.1016/j.surfcoat.2015.09.047.
6. Jelil RA. A review of low-temperature plasma treatment of textile materials. J Mater Sci. 2015;50:5913-43. http://doi.org/10.1007/s10853-015-9152-4.
7. Radetic M, Jovancic P, Puac N, Petrovic ZL. Environmental impact of plasma application to textiles. J Phys Conf Ser. 2007;71(1):012017. http://doi.org/10.1088/1742-6596/71/1/012017.
8. Samanta K, Jassa M, Agrawal AK. Atmospheric pressure glow discharge plasma and its applications in textile. Indian J Fibre Text Res. 2006;31:83-98.
9. Kale KH, Palaskar S. Atmospheric pressure plasma polymerization of hexamethyldisiloxane for imparting water repellency to cotton fabric. Text Res J. 2011;81(6):608-20. http://doi.org/10.1177/0040517510385176.
10. Mariotti D, Belmonte T, Benedikt J, Velusamy T, Jain G, Švrček V. Low-temperature atmospheric pressure plasma processes for 'green' third generation photovoltaics. Plasma Process Polym. 2016;13(1):70-90. http://doi.org/10.1002/ppap.201500187.
11. Nema SK, Jhala PB. Plasma technologies for textile and apparel. New Delhi: Woodhead Publishing India; 2015.
12. Morent R, De Geyter N, Verschuren J, De Clerck K, Kiekens P, Leys C. Non-thermal plasma treatment of textiles. Surf Coat Tech. 2008;202(14):3427-49. http://doi.org/10.1016/j.surfcoat.2007.12.027.
13. Coopes IH, Gifkins KJ. Gas plasma treatment of polymer surfaces. J Macromol Sci Chem. 1982;17(2):217-26. http://doi.org/10.1080/00222338208063256.
14. Caiazzo F, Canonico P, Nigro R, Tagliaferri V. Electrode discharge for plasma surface treatment of polymeric materials. J Mater Process Technol. 1996;58(1):96-9. http://doi.org/10.1016/0924-0136(95)02112-4.
15. Gasi F, Petraconi G, Bittencourt E, Lourenço SR, Castro AHR, Miranda FS, et al. Plasma treatment of polyamide fabric surface by hybrid corona-dielectric barrier discharge: material characterization and dyeing/washing processes. Mater Res. 2020;23(1):e20190255. http://doi.org/10.1590/1980-5373-mr-2019-0255.
16. Bruggeman PJ, Iza F, Brandenburg R. Foundations of atmospheric pressure non-equilibrium plasmas. Plasma Sources Sci Technol. 2017;26(12):123002. http://doi.org/10.1088/1361-6595/aa97af.
17. Hegemann D. Plasma polymerization and its application in textiles. Indian J Fibre Text Res. 2006;31(1):99-115.
18. Fracassi F, d'Agostino R, Fanelli F, Fornelli A, Palumbo F. GC-MS investigation of hexamethyldisiloxane-oxygen fed plasmas. Plasma Polym. 2003;8(4):259-69. http://doi.org/10.1023/A:1026333126452.

19. Fanelli F, Lovascio S, D'Agostino R, Fracassi F. Insights into the atmospheric pressure plasma-enhanced chemical vapor deposition of thin films from methyldisiloxane precursors. Plasma Process Polym. 2012;9(11-12):1132-43. http://doi.org/10.1002/ppap.201100157.
20. Cacot L, Carnide G, Kahn ML, Clergereaux R, Naudé N, Stafford L. Kinetics driving thin-film deposition in dielectric barrier discharges using a direct liquid injector operated in a pulsed regime. J Phys D Appl Phys. 2022;55(47):475202. http://doi.org/10.1088/1361-6463/ac94de.
21. Petraconi A, Miranda F, Prado E, Braite B, Gasi F, Bittencourt E, et al. Hybrid corona-dielectric barrier discharge for permethrin polymerisation on polyamide fabric at atmospheric pressure. Fibers Polym. 2023;24(2):373-82. http://doi.org/10.1007/s12221-023-00058-2.
22. Bogaerts A, Tu X, Whitehead JC, Centi G, Lefferts L, Guaitella O, et al. The 2020 plasma catalysis roadmap. J Phys D Appl Phys. 2020;53(44):443001. http://doi.org/10.1088/1361-6463/ab9048.
23. Nguyen DB, Lee WG. Effects of ambient gas on cold atmospheric plasma discharge in the decomposition of trifluoromethane. RSC Advances. 2016;6(32):26505-13. http://doi.org/10.1039/C6RA01485B.
24. Miranda FS, Caliari FR, Campos TM, Leite DMG, Pessoa RS, Essiptchouk AM, et al. High-velocity plasma spray process using hybrid SiO_2 + ZrO_2 precursor for deposition of environmental barrier coatings. Surf Coat Tech. 2020;404:126447. http://doi.org/10.1016/j.surfcoat.2020.126447.
25. Bertran CA, Silva NT, Thim GP. Citric acid effect on aqueous sol-gel cordierite synthesis. J Non-Cryst Solids. 2000;273(1-3):140-4. http://doi.org/10.1016/S0022-3093(00)00157-5.
26. Ribas RG, Campos TMB, Schatkoski VM, Menezes BRC, Montanheiro TLA, Thim GP. α-wollastonite crystallization at low temperature. Ceram Int. 2020;46(5):6575-80. http://doi.org/10.1016/j.ceramint.2019.11.143.
27. Nascimento L, Gasi F, Landers R, da Silva Sobrinho A, Aragão E, Fraga M, et al. Physicochemical studies on the surface of polyamide 6.6 fabrics functionalized by DBD plasmas operated at atmospheric and sub-atmospheric pressures. Polymers. 2020;12(9):2128. http://doi.org/10.3390/polym12092128.
28. Gerullis S, Pfuch A, Spange S, Kettner F, Plaschkies K, Küzün B, et al. Thin antimicrobial silver, copper or zinc containing SiOx films on wood polymer composites (WPC) applied by atmospheric pressure plasma chemical vapour deposition (APCVD) and sol–gel technology. Holz Roh- Werkst. 2018;76(1):229-41. http://doi.org/10.1007/s00107-017-1220-9.
29. Montarsolo A, Mossotti R, Innocenti R, Vassallo E. A study on washing resistance of pp-HMDSO films deposited on wool fabrics for anti-pilling purposes. Surf Coat Tech. 2013;224:109-13. http://doi.org/10.1016/j.surfcoat.2013.03.007.
30. Hegemann D. Plasma polymer deposition and coatings on polymers. Compr Mater Process. 2014;4:201-28. http://doi.org/10.1016/B978-0-08-096532-1.00426-X.
31. Profili J, Levasseur O, Blaisot JB, Koronai A, Stafford L, Gherardi N. Nebulization of nanocolloidal suspensions for the growth of nanocomposite coatings in dielectric barrier discharges. Plasma Process Polym. 2016;13(10):981-9. http://doi.org/10.1002/ppap.201500223.
32. Zille A, Fernandes MM, Francesko A, Tzanov T, Fernandes M, Oliveira FR, et al. Size and aging effects on antimicrobial efficiency of silver nanoparticles coated on polyamide fabrics activated by atmospheric DBD Plasma. ACS Appl Mater Interfaces. 2015;7(25):13731-44. http://doi.org/10.1021/acsami.5b04340.
33. Zhang W, Dehghani-Sanij AA, Blackburn RS. IR study on hydrogen bonding in epoxy resin-silica nanocomposites. Prog Nat Sci. 2008;18(7):801-5. http://doi.org/10.1016/j.pnsc.2008.01.024.
34. Subedi DP, Joshi UM, Wong CS. Dielectric barrier discharge (DBD) plasmas and their applications. In: Rawat RS, editor. Plasma science and technology for emerging economies: an AAAPT experience. Singapore: Springer; 2017. p. 693-737. http://doi.org/10.1007/978-981-10-4217-1_13.
35. van der Mei HC, Stokroos I, Schakenraad JM, Busscher HJ. Aging effects of repeatedly glow-discharged polyethylene: influence on contact angle, infrared absorption, elemental surface composition, and surface topography. J Adhes Sci Technol. 1991;5(9):757-69. http://doi.org/10.1163/156856191X00684.
36. Canal C, Molina R, Bertran E, Erra P. Wettability, ageing and recovery process of plasma-treated polyamide 6. J Adhes Sci Technol. 2004;18(9):1077-89. http://doi.org/10.1163/1568561041257487.
37. Basu BJ, Hariprakash V, Aruna ST, Lakshmi RV, Manasa J, Shruthi BS. Effect of microstructure and surface roughness on the wettability of superhydrophobic sol-gel nanocomposite coatings. J Sol-Gel Sci Technol. 2010;56(3):278-86. http://doi.org/10.1007/s10971-010-2304-8.
38. García-Pérez C, Menchaca-Campos C, García-Sánchez MA, Pereyra-Laguna E, Rodríguez-Pérez O, Uruchurtu-Chavarín J. Nylon/porphyrin/graphene oxide fiber ternary composite, synthesis and characterization. Open Journal of Composite Materials. 2017;7(3):146-65. http://doi.org/10.4236/ojcm.2017.73009.